Regional Aerosol Retrieval Results From MISR

John V. Martonchik, *Associate Member, IEEE*, David J. Diner, *Associate Member, IEEE*, Kathleen A. Crean, and Michael A. Bull

***Abstract*—Examples of aerosol retrieval results, derived from the Multi-angle Imaging SpectroRadiometer (MISR) on the Earth Observation Science (EOS) Terra platform, are shown and the performance of the retrieval algorithms are discussed, following the first 18 months of operational data processing. A number of algorithm modifications were implemented, based on an analysis of aerosol retrieval results during this period, and these changes are described. Two cloud-screening algorithms, the angle-to-angle smoothness and angle-to-angle correlation tests, which were used in the preprocessing phase of the analyses are also described. The aerosol retrieval examples cover a wide variety of conditions, both over land and water. Particular aerosol types include dust clouds, forest fire and volcanic plumes, and localized dense haze. Finally, some ideas are discussed for additional improvement of the MISR aerosol data product, based on the experience gained in analyzing multiangle data and the associated geophysical products.**

***Index Terms*—Aerosol, algorithms, remote sensing.**

I. Introduction

THE Multi-angle Imaging SpectroRadiometer (MISR) on the Earth Observation Science (EOS) Terra platform has been operational since late February 2000. The instrument's typical data collection mode is to observe the earth globally at nine different view zenith angles, ranging from 70° forward to 70° aftward along the spacecraft track, in four spectral bands (446, 558, 672, and 866 nm) and with a crosstrack ground spatial resolution of 275 m–1.1 km and a swathwidth of 400 km [1]. After these 36 channels of imaging data are radiometrically calibrated, georectified, and averaged to a uniform resolution of 1.1 km, they then are analyzed to determine aerosol properties over both land and ocean at a resolution of 17.6 km × 17.6 km. All routine operational processing of MISR data and subsequent product archiving is carried out at the NASA Langley Atmospheric Science Data Center (ASDC).

The aerosol retrieval methodologies being used with MISR data have been described by Martonchik *et al.* [2] and are summarized in Fig. 1. Implementation of both the land (Heterogeneous Land) and ocean (Dark Water) aerosol retrieval algorithms require a predetermined set of aerosol models and their associated radiative atmospheric parameters, in particular the atmospheric path radiance and, over water, the upward transmittance of surface-reflected radiance. These parameters have been calculated for selected aerosol types with monomodal particle size distributions and are stored as a function of angular geometry and aerosol amount in various lookup tables as part of the Simulated MISR Ancillary Radiative Transfer (SMART) dataset [2]. Mixtures of two or three aerosol types produce a wide variety of aerosol models described by bimodal or trimodal size distributions [2], and these mixture models are the ones used by the MISR aerosol retrieval algorithms. The necessary radiative atmospheric parameters for these mixture models are created from the aerosol data during the actual retrieval process, using a modified linear mixing theory [3]. This strategy provides a large set of aerosol models for use in the retrieval analysis while keeping the SMART dataset at a manageable size.

In this paper, we describe the current state of the MISR Heterogeneous Land and Dark Water aerosol retrieval algorithms, emphasizing the rationale for several modifications of the algorithms that have been made during the relatively short period since MISR achieved operational status. Then, aerosol retrieval results are shown over both land and ocean for a variety of aerosol conditions, ranging from background aerosols and concentrated fogs to dust clouds, wildfire, and volcanic plumes. Finally, we discuss the need for and the direction of future modifications to the MISR aerosol retrieval process, starting with the selection of the aerosol types in the SMART dataset and following through to the criteria which define the basic operation of the algorithms. This need for ongoing change is a response to our ongoing assessment of the quality of the MISR aerosol retrieval results and our increased understanding and appreciation of the informational content of multiangle imagery.

II. Algorithm Modifications

A few important changes have been made to some of the operational aspects of the MISR aerosol retrieval algorithms, which were originally described in [2]. First and foremost is the deletion of the Dense Dark Vegetation (DDV) Algorithm as an operational aerosol retrieval algorithm at the Langley ASDC. Its purpose was to be another option, along side the Heterogeneous Land Algorithm outlined in Fig. 1, for performing a retrieval over land when dense, dark vegetation was present. As such, its applicability in any geographic area was limited in extent, unlike the Heterogeneous Land Algorithm which requires only a reasonable amount of scene contrast within the aerosol retrieval region. In fact, results from the current Heterogeneous Land Algorithm have demonstrated that it works well over DDV regions, making unnecessary the need for an alternative DDV-specific algorithm.

The Heterogeneous Land Algorithm has been modified somewhat from the original operational version available at launch

Manuscript received October 7, 2001; revised April 22, 2002. The research described in this paper was carried out at the Jet Propulsion Laboratory, California Institute of Technology, under a contract with the National Aeronautics and Space Administration.

The authors are with the Jet Propulsion Laboratory, California Institute of Technology, Pasadena, CA 91109 USA (e-mail: jvm@jord.jpl.nasa.gov).

Publisher Item Identifier 10.1109/TGRS.2002.801142.

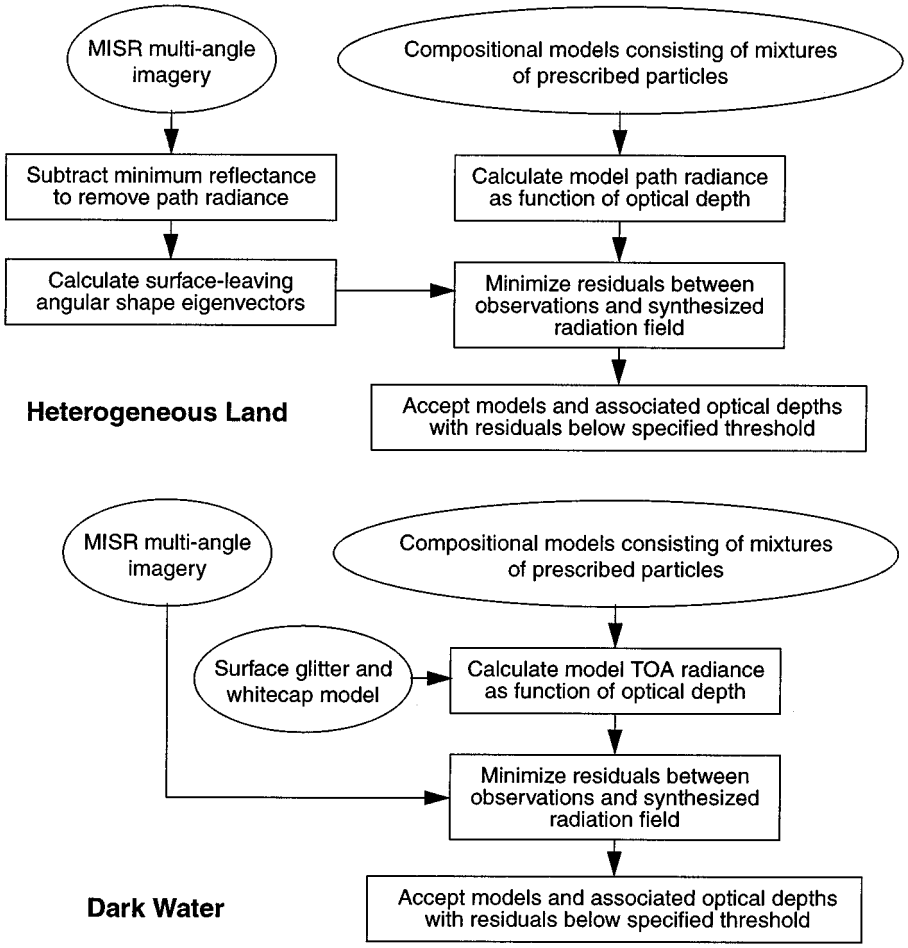

Fig. 1. Schematics of MISR Heterogeneous Land aerosol retrieval algorithm (top) and Dark Water aerosol retrieval algorithm (bottom).

time. This original version, described in [2], used the average of the MISR radiances over the 16×16 1.1-km pixels in the 17.6 km $\times$ 17.6 km region of interest to construct the 9×9 element scatter matrix C

$$C_{ij} = \sum_{x,y} \left[L_{x,y}^{\mathrm{MISR}}(i) - \left\langle L^{\mathrm{MISR}}(i)\right\rangle\right] \cdot \left[L_{x,y}^{\mathrm{MISR}}(j) - \left\langle L^{\mathrm{MISR}}(j)\right\rangle\right]. \quad (1)$$

Here $L_{x,y}^{\mathrm{MISR}}$ is the MISR radiance at pixel location x, y within the region, $\left\langle L^{\mathrm{MISR}}\right\rangle$ is the average radiance of the 16×16 pixels within the region, i and j are indices which designate a particular MISR camera view, and the summation is over the 256 pixels within the region. In (1) and subsequent expressions, the explicit dependence on wavelength of radiance is not shown for brevity. The subtraction process expressed in (1) removes completely any effect of the atmospheric path radiance (an additive term in the expression describing $L_{x,y}^{\mathrm{MISR}}$), assuming that the atmosphere is laterally homogeneous within the region. Then the eigenvectors and eigenvalues of matrix C are used to express that component of the MISR radiances which is directly and diffusely transmitted from the surface. The retrieval algorithm has been modified by redefining the scatter matrix C, whereby the camera-dependent average radiances $\left\langle L^{\mathrm{MISR}}\right\rangle$ were replaced with the camera-dependent radiances $L_{\mathrm{darkest}}^{\mathrm{MISR}}$ of the pixel which is darkest in the nadir view camera, i.e.,

$$C_{ij} = \sum_{x,y} \left[L_{x,y}^{\mathrm{MISR}}(i) - L_{\mathrm{darkest}}^{\mathrm{MISR}}(i)\right] \cdot \left[L_{x,y}^{\mathrm{MISR}}(j) - L_{\mathrm{darkest}}^{\mathrm{MISR}}(j)\right]. \quad (2)$$

This modification was driven by the fact that the MISR radiances can be expressed as

$$L_{x,y}^{\mathrm{MISR}}(i) = L_{\mathrm{bias}}^{\mathrm{MISR}}(i) + \sum_n A_n^{x,y} f_n(i) \quad (3)$$

where $L_{\mathrm{bias}}^{\mathrm{MISR}}$ is either $\left\langle L^{\mathrm{MISR}}\right\rangle$ when (1) is used or $L_{\mathrm{darkest}}^{\mathrm{MISR}}$ when (2) is used, f_n are the associated eigenvectors, and $A_n^{x,y}$ are the expansion coefficients. The Heterogeneous Land Algorithm uses the region-averaged MISR radiances,

$$\begin{aligned}\left\langle L^{\mathrm{MISR}}(i)\right\rangle &= L_{\mathrm{bias}}^{\mathrm{MISR}}(i) + \sum_n \left\langle A_n\right\rangle f_n(i) \\ &= L^{\mathrm{apr}}(i) + L_{\mathrm{bias,surf}}^{\mathrm{MISR}}(i) + \sum_n \left\langle A_n\right\rangle f_n(i) \\ &= L_{\mathrm{model}}^{\mathrm{apr}}(i) + \sum_n B_n f_n(i) \end{aligned} \quad (4)$$

where L^{apr} is the atmospheric path radiance and $L_{\mathrm{bias,surf}}^{\mathrm{MISR}}$ is the surface-leaving radiance contribution to $L_{\mathrm{bias}}^{\mathrm{MISR}}$. The

region-averaged MISR radiances on the left side of the equation is compared, via least squares, to the expression on the right side which is composed of $L^{\mathrm{apr}}_{\mathrm{model}}$, the atmospheric path radiance for a particular aerosol model, and an eigenvector expansion with best fit coefficients B_n. All aerosol models that produce a quality of fit within a specified threshold are considered to be a successful retrieval. Note that $L^{\mathrm{MISR}}_{\mathrm{bias,surf}}$ is subsumed into the expansion term, under the assumption that it can be adequately represented by the eigenvectors. From looking at numerous examples of aerosol retrievals and comparing results obtained using (1) with those using (2), it was clear that selecting the dark pixel radiances as the bias radiances, i.e., (2), resulted in a greater quantity of successful retrievals. This is explained by the fact that, in general, fewer eigenvectors are needed in the expansion in (4) when $L^{\mathrm{MISR}}_{\mathrm{bias}} = L^{\mathrm{MISR}}_{\mathrm{darkest}}$ than when $L^{\mathrm{MISR}}_{\mathrm{bias}} = \langle L^{\mathrm{MISR}} \rangle$, making the algorithm inherently more sensitive. Also, since $L^{\mathrm{MISR}}_{\mathrm{bias,surf}}$ is smaller when it is associated with the darkest pixel rather than the average pixel, the accuracy of its representation in the expansion in (4) is less important.

Another modification applied to both the Heterogeneous Land and the Dark Water Algorithm is a redefinition of the various χ^2 tests used to find the best fitting aerosol models. The original χ^2 expressions (absolute, spectral, geometric, and maximum deviation) for the Dark Water Algorithm [2] used variances, which were based on absolute radiometric uncertainties of the MISR instrument. However, this was determined to be too restrictive, since the limited number of aerosol models used in the analyses did not have the necessary flexibility to fit the measurements to that required accuracy. The Heterogeneous Land Algorithm had a similar problem with the variance in its χ^2 expression. Here, the variance was a function of the sum of eigenvalues of those eigenvectors which are ignored in the expansion of (4) [2]. This eigenvalue sum can be considered a noise factor, but again its use as the variance proved to be too restrictive in the retrieval process. Thus, a new variance criterion, applicable to both the Dark Water Algorithm and the Heterogeneous Land Algorithm, was selected which makes use of only the MISR measurements. Simply stated, the uncertainty $(\sqrt{\mathrm{variance}})$ for any of the χ^2 expressions now is a constant fraction of the particular measurement (e.g., radiances or ratios of radiances) being fitted. The constant fraction is a configurable parameter currently set at 0.05. This modification to the algorithms has resulted in a substantial increase in the number of successful retrievals both over land and ocean, compared to the initial retrieval success rate immediately after launch.

Finally, some effort was made to fill in regional "holes" where the aerosol retrieval attempts were unsuccessful. This procedure is especially important over land, since no subsequent surface retrieval can be performed in a region lacking an adequate characterization of the overlying atmosphere. Therefore, a simple scheme was implemented whereby the unsuccessful region was assigned a default optical depth equal to the average optical depth of all successful retrievals in a domain nearby the domain containing the unsuccessful region. A domain is a standard MISR unit of area, defined as a 4×4 array of regions (70.6 km $\times$ 70.6 km), in which all aerosol and surface retrieval are performed before moving to the next domain. Under many conditions aerosol characteristics will vary little between adjacent domains, so this approximate (default) characterization of the atmosphere in a failed region will allow a reasonably accurate surface properties retrieval to be performed. However, the default fill procedure as currently implemented, allows the possibility of propagating a particular default optical depth into regions quite far from the domain where the default optical depth originated, a deficiency to be corrected in the next software upgrade. The status of the aerosol retrieval (successful, default, or no retrieval) for each region is archived in the MISR aerosol product.

For more information on the MISR aerosol retrieval algorithms, documentation can be found at http://eospso.gsfc.nasa.gov/atbd/misrtables.html.

III. Cloud Screening

Before any aerosol retrievals are performed using MISR data, the imagery is first put through a cloud-screening process. This process identifies all areas in a scene that are considered not suitable for an aerosol/surface retrieval. Currently, two tests are performed including a radiance angle-to-angle smoothness evaluation and an image angle-to-angle correlation. Each is used with Level 1B2 MISR data, i.e., multiangle imagery that has been radiometrically calibrated, coregistered, and geolocated to the terrain or ocean surface. As such, if there are any clouds occurring within a scene, they will appear to be misregistered because of parallax. Since these two tests are designed to detect any such misregistrations, they provide some measure of cloud screening.

A. Radiance Angle-to-Angle Smoothness Evaluation

This is a test to insure that the MISR measurements for each 1.1-km subregion are "smooth" as a function of camera angle. If a particular pixel location in the imagery is contaminated by clouds, different camera views of that pixel will not see the same cloud element, most likely causing a nonsmooth appearance of the angular signature of the radiances associated with that pixel location. For each spectral band this test is performed twice, once used with the forward plus nadir camera dataset (five angles) and then with the aftward plus nadir camera dataset (five angles). Failure of the smoothness test for either dataset in any band causes that subregion to be eliminated from the aerosol retrieval process.

The measurements of each of the two datasets are fitted to a polynomial with one less degree of freedom than the number of cameras. Thus, the full complement of five cameras (four aftward or four forward view plus nadir view) in a dataset would be fitted by a cubic polynomial. Over water, the use of less than five cameras frequently occurs due to glitter, and if fewer than four cameras are used, this test is not performed. For each dataset the smoothness test parameter χ^2_{smooth} is calculated as

$$\chi^2_{\mathrm{smooth}} = \frac{1}{N_{\mathrm{cam}}} \cdot \sum_{k=1}^{N_{\mathrm{cam}}} \frac{\left[L^{\mathrm{MISR}}_{x,y}(k) - L^{\mathrm{poly}}(k)\right]^2}{\sigma^2_{\mathrm{smooth}}(k)} \quad (5)$$

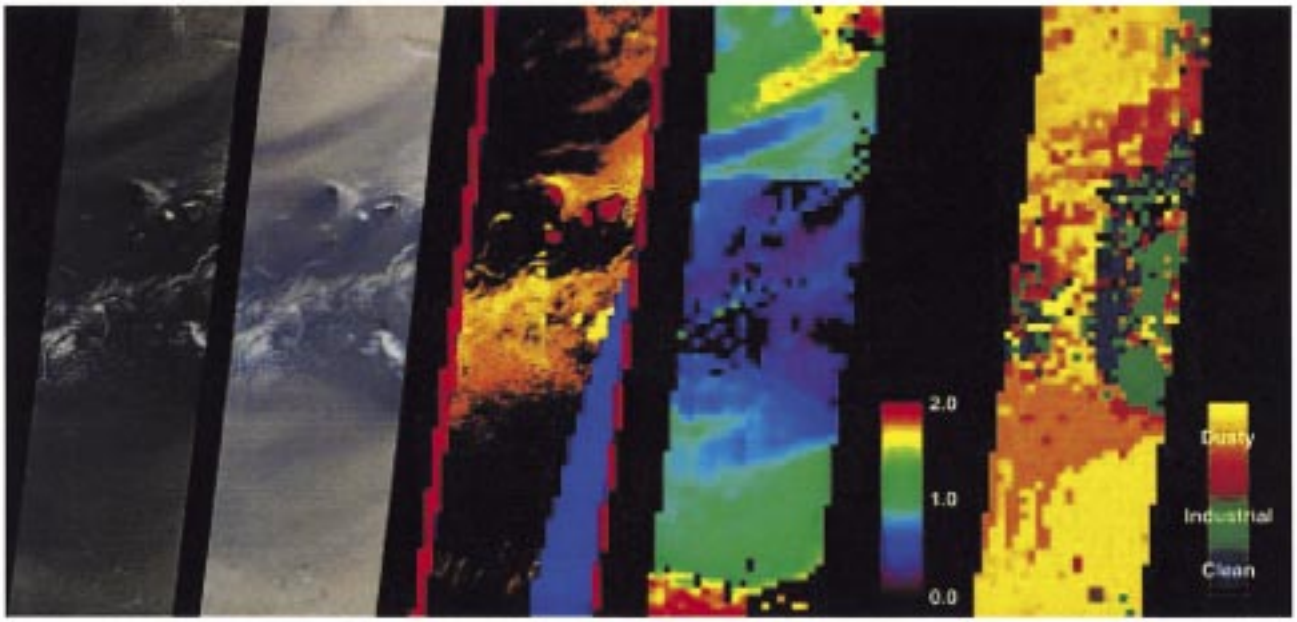

Fig. 2. Dust storm over the Canary Islands on February 29, 2000. Swath segments (path 208, orbit 1065) shown (left to right) are: true-color TOA nadir view, TOA 70° aftward view, nadir camera retrieval applicability mask (see text for details), retrieved aerosol optical depth (558 nm), best fit aerosol model.

where $L_{x,y}^{\mathrm{MISR}}$ are the MISR measurements at pixel location x, y, L^{poly} are the corresponding least squares polynomial fits, σ_{smooth} is the acceptable goodness of fit defined to be equal to $0.03L_{x,y}^{\mathrm{MISR}}$, and N_{cam} is the number of usable camera views. Failure of the smoothness test occurs when χ^2_{smooth} is greater than a specified limit. Nonperformance of the test, due to an insufficient number of cameras, results in an automatic passing of the test.

B. Image Angle-to-Angle Correlation

The angle-to-angle correlation test is designed to detect features, which result in poor correlation of the radiance spatial distribution from one view angle to another, e.g., a cloud within a subregion. This test makes use of the MISR 275-m radiance data, routinely available in the red band for all camera views, and producing a 4×4 array of radiances for each 1.1-km subregion. A poor correlation results in that subregion being eliminated from the aerosol retrieval process.

The first step is to generate a camera-averaged "template" 4×4 image from the 275 m red band data

$$L_{\mathrm{temp}}^{\mathrm{MISR}}(i,j) = \frac{1}{N_{\mathrm{cam}}} \cdot \sum_{k=1}^{N_{\mathrm{cam}}} L_{275,\mathrm{red}}^{\mathrm{MISR}}(i,j;k) \tag{6}$$

where i, j are the indices of the 4×4 array, k designates a particular camera view, and N_{cam} is the total number of cameras used. The correlation is then computed between the 4×4 subregion image of each camera to the template image. For each camera, the variance and covariance are calculated as follows:

$$\begin{aligned}
\sigma^2_{\mathrm{corr}}(k) &= \left\langle \left[L_{275,\mathrm{red}}^{\mathrm{MISR}}(k)\right]^2 \right\rangle - \left\langle L_{275,\mathrm{red}}^{\mathrm{MISR}}(k) \right\rangle^2 \\
\sigma^2_{\mathrm{temp}} &= \left\langle \left[L_{\mathrm{temp}}^{\mathrm{MISR}}\right]^2 \right\rangle - \left\langle L_{\mathrm{temp}}^{\mathrm{MISR}} \right\rangle^2 \\
\sigma^2(k) &= \left\langle L_{\mathrm{temp}}^{\mathrm{MISR}} L_{275,\mathrm{red}}^{\mathrm{MISR}}(k) \right\rangle - \left\langle L_{\mathrm{temp}}^{\mathrm{MISR}} \right\rangle \left\langle L_{275,\mathrm{red}}^{\mathrm{MISR}}(k) \right\rangle
\end{aligned} \tag{7}$$

where the angle brackets indicate a spatial average, computed over the 4×4 array of pixels.

Then, the square of the normalized cross correlation is calculated as

$$C(k) = \frac{\sigma^2(k)|\sigma^2(k)|}{\sigma^2_{\mathrm{temp}}\sigma^2_{\mathrm{corr}}(k)}. \tag{8}$$

Note that the sign of the covariance between the two windows is preserved in (8). If there is a high correlation between the radiance distribution of camera k and the template, C will take on values close to 1. Anticorrelation results in negative values of C. The criterion for accepting a camera in the aerosol retrievals is that the value of C must exceed a threshold value C_{thresh}. This threshold value is currently set to 0.25 based on experience using in-flight data. If the test fails for any camera, the entire subregion is eliminated from the retrieval process. Note that if the denominator of (8) is zero or close enough to zero to cause a computational problem (this can occur if the radiance distributions are uniform), the correlation test is considered to be passed for those affected cameras.

IV. Retrieval Examples

MISR aerosol retrievals are routinely performed at the Langley ASDC, encountering a wide variety of atmospheric situations. Here, a selected number of retrieval cases are presented (software version 2.1.3), illustrating some of these varied aerosol conditions and also introducing various elements of the MISR aerosol standard product. These retrieval case examples typically have an areal expanse covering the full width of the MISR swath (about 400 km east–west) and extending north–south about 1400 km along the orbital path, a size large enough to display the atmospheric features of interest.

A. Dust Storm Over the Canary Islands

When MISR observed the Canary Islands on February 29, 2000 (path 208, orbit 1065), a large dust cloud, sweeping off the northwestern African coast, was engulfing the islands and surrounding area. Fig. 2 shows true-color (red, green, blue band composite) swath segments for the nadir viewing (far left) and 70° aftward viewing (left) cameras, illustrating the considerable increase in dust cloud brightness at large view angles as compared to nadir. This phenomenon is typically encountered in MISR imagery, a consequence of the larger aerosol path length observed with increasing view angle.

The middle-swath segment shows the nadir camera retrieval applicability mask, designating which pixels are suitable for use in the retrieval process. Computed for each camera, this mask incorporates the failure results generated by the angle-to-angle smoothness test (orange pixels) and correlation test (yellow pixels), along with the failure results from a glitter test (blue pixels) and a topographic complexity/missing data test (red pixels). Note that the individual islands, displayed in red in the middle of the swath segment, are classified as being topographically complex and are not used in an aerosol retrieval. Only the black pixels in the mask are deemed usable. Comparison of this mask with the corresponding imagery on the left indicates that the various screening tests employed in the preprocessing step of the analysis, have done a reasonable job in detecting the spatially variable condensate cloud regions while passing the more spatially uniform dust cloud regions, which are suitable for an aerosol retrieval.

The next swath segment on the right side of Fig. 2 shows the retrieved aerosol optical depth at 558 nm (MISR green band), with values ranging from 0.2 to 2.0. The noticeable square elements in the optical depth map are a manifestation of the 17.6 km $\times$ 17.6 km resolution criterion, employed by the retrieval algorithm. Those areas colored black indicate that no aerosol retrieval results are available, either because the multicamera retrieval applicability masks excluded them or because the retrieval was unsuccessful at finding an aerosol model that satisfied the χ^2 criteria. Note that there are successful retrievals in areas of the swath segment where the mask indicates that clouds appear to be present. This is especially apparent on the far right of the swath segment toward the middle, where a band of clouds crosses the image. Recalling that the mask is generated at 1.1-km resolution while the retrieval is performed on a scale of 17.6 km, the Dark Water aerosol retrieval algorithm (see Fig. 1) will search for any available 1.1-km pixels which pass the cloud-screening tests out of the 256 pixels contained within the region of the retrieval. If only one good pixel is present, it will be used in the retrieval process and the results applied to the entire 17.6 km $\times$ 17.6 km region. This criterion of "just a single clear pixel between the clouds" seems not to be unreasonable when using the Dark Water Algorithm, since there appears to be no effect from clouds in the resulting optical depth map. Likewise, the nadir camera retrieval applicability mask shows significant glitter effects in the lower right side of the swath segment, making the nadir camera unusable. However, there are other MISR cameras where glitter is not a problem in this region, allowing a successful aerosol retrieval to be performed as indicated in the optical depth map.

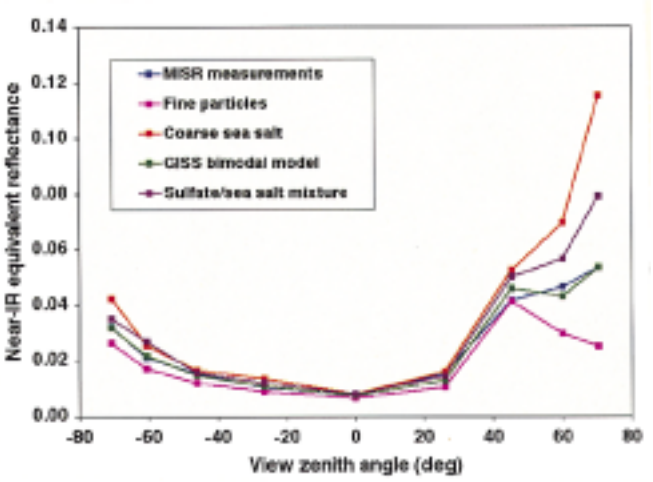

Fig. 3. MISR band 4 equivalent reflectance versus camera view angle for an ocean location off the coast of southern Africa on August 27, 2000. Also shown are results from four aerosol models assuming a surface windspeed of 3.4 m/s. The scattering angles of the observations range from 166° (the backward scattering view at −46°) to 61° (the forward scattering view at 70°).

Finally, the swath segment on the far right of the figure indicates the type of aerosol which best fitted the MISR measurements. The 49 aerosol models used in the MISR operational retrievals over ocean are grouped under three broad categories: clean, industrial, and dusty maritime. The 14 models classified as clean maritime are mixtures composed of various amounts of three basic particle types, namely accumulation mode sulfate/nitrate particles and accumulation and coarse mode sea salt particles. The 12 industrial maritime models are similar to the clean models but with black carbon replacing the coarse mode sea salt. The third group, dusty maritime, can be split into two subgroups of dusty aerosol models. The 18 models in the first subgroup are similar to the clean maritime models but with high-altitude medium-size dust replacing the coarse sea salt. The five models in the remaining subgroup are composed only of dust particles, namely low-altitude medium and large dust particles and high-altitude medium-size dust particles. In the aerosol type map of Fig. 2, the three categories of aerosol models can be identified, but the dusty maritime models clearly dominate the scene. Over ocean, the MISR instrument is quite sensitive to nonspherical particles such as dust [4], so it is encouraging that, under obviously dusty conditions, the dust-based models are the best fitting models.

B. Aerosol Retrieval off the Coast of South Africa

The success of MISR aerosol retrievals over ocean has proven to be very sensitive to the selected aerosol models being employed. In particular, for MISR the particle shape and size distribution are the most important aspects describing an aerosol model; sensitivity to the refractive index is much lower [5]. Fig. 3 shows an example of MISR measurements at the nine camera view angles in the near-infrared band (866 nm) for a cloud-free location about 50 km off the southern coast of South

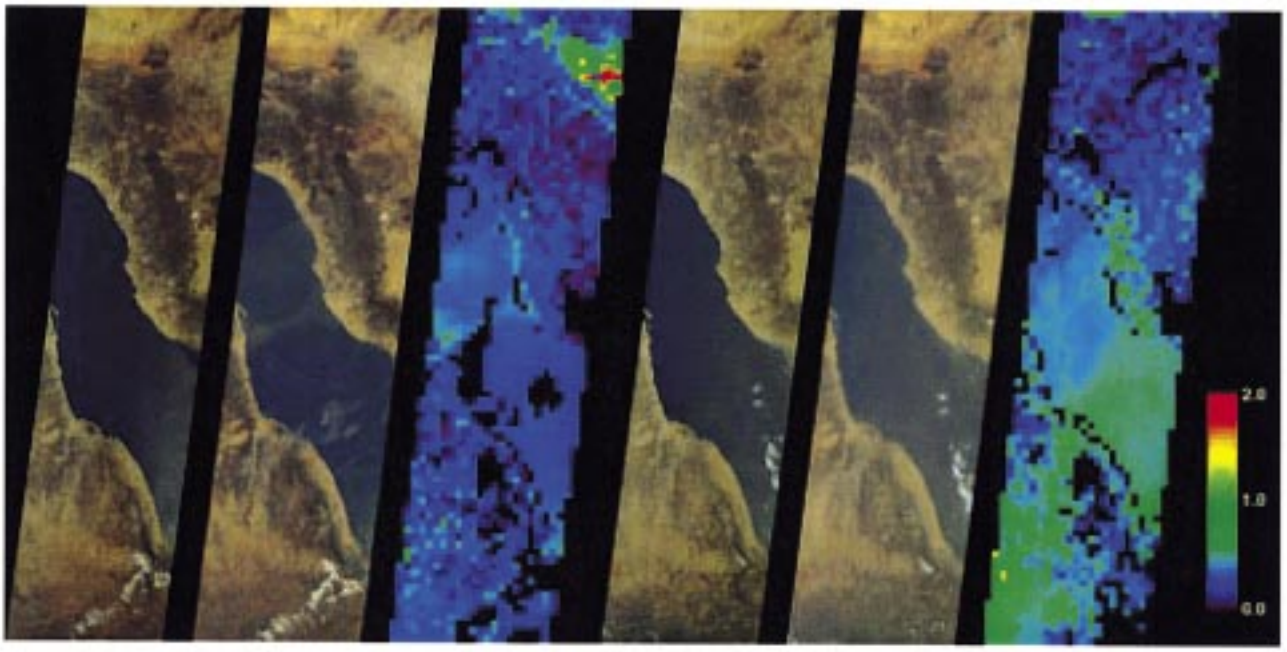

Fig. 4. Dust clouds over the Red Sea. Swath segments shown (left to right) March 25, 2001 (path 170, orbit 6742) are: true-color TOA nadir view, TOA 70° forward view, retrieved aerosol optical depth (558 nm), June 29, 2001 (path 170, orbit 8140) true-color TOA nadir view, TOA 70° forward view, retrieved aerosol optical depth (558 nm).

Africa on August 27, 2000 (path 172, orbit 3684). This particular case is interesting in that all 49 ocean aerosol models used in the MISR operational retrieval process were unsuccessful in fitting these data. This is not an isolated case, but is representative of a fairly large number of situations encountered around the globe where MISR ocean aerosol retrievals failed to find a successful model within the preestablished lookup dataset.

Also shown in the figure are three examples (fine particles, sulfate/sea salt mixture, coarse sea salt) of efforts to fit the measurements using different types of aerosol models, characterized mainly by their particle size. The fine particles and coarse sea salt particles are described by monomodal log normal size distributions with similar widths but having vastly different effective radii [6], 0.003 μm for the fine particles and 17 μm for the coarse sea salt. The bimodal sulfate/sea salt mixture (one of the MISR clean maritime models) is composed of 80% sulfate/nitrate (0.3-μm effective radius) and 20% sea salt (1.20 μm), as measured by optical depth at 558 nm, and representing a medium particle size model between the fine particle and coarse sea salt. All models required a small optical depth ($\leq$0.075 at 558 nm) for their best fit of the measurements, but each shows large deviations from the measurements at large forward viewing angles (positive view zenith angle in Fig. 3). Normalizing all results to the nadir view, there is a systematic trend of the smallest particles to undershoot the measurements and the largest particles to overshoot them. Note that the measurements for the 46° and 60° forward view cameras are contaminated by glint, while the most forward viewing camera at 70° is not. The data from these two glint-contaminated cameras would not normally be used in the MISR retrieval, but it is instructive to note that these measurements could be modeled using the Cox–Munk theory [7] with surface windspeed as a parameter to be determined.

The last curve in the figure (labeled the GISS bimodal model) represents an aerosol model, recently derived from aircraft photopolarimeter measurements off the coast of Monterey, CA [8]. Interestingly, this model best fits the MISR measurements for this southern Africa oceanic case study. It is composed of fine (water soluble) and coarse (sea salt) mode particles with effective radii of 0.1 and 1.0 μm, respectively, and with a mixture ratio such that the fine mode contributes about 60% of the optical depth at 558 nm. None of the current MISR maritime aerosol models has a component composed of particles as small as the fine mode of the GISS (Goddard Institute for Space Studies) model. Indeed, the smallest effective radius in the SMART dataset is 0.21 μm, a condition which is believed to account for the inability to adequately fit the measurements in many cases. However, it is by looking at failures in the ocean retrievals, such as illustrated in Fig. 3, that reveal deficiencies in the current algorithm and its associated aerosol dataset and point the way to improvements required to resolve them.

C. Dust Clouds Over the Red Sea

Fig. 4 shows swath segments of a portion of the Middle East with Saudi Arabia at the top of the images, Sudan, Eritrea, and Ethiopia toward the bottom, and the Red Sea cutting through the center. The first three swath segments on the left side of the figure used measurements taken on March 25, 2001 (path 170, orbit 6742), displaying the true-color nadir view, 70° forward view, and retrieved optical depth, respectively. The second set of three swath segments on the right of the figure has identical characteristics as the first, but used measurements taken on June 29, 2001 (path 170, orbit 8140), three months later. Like the Canary Island scene, the 70° view images for both dates accentuate the dust clouds over the water, as compared with their nadir view

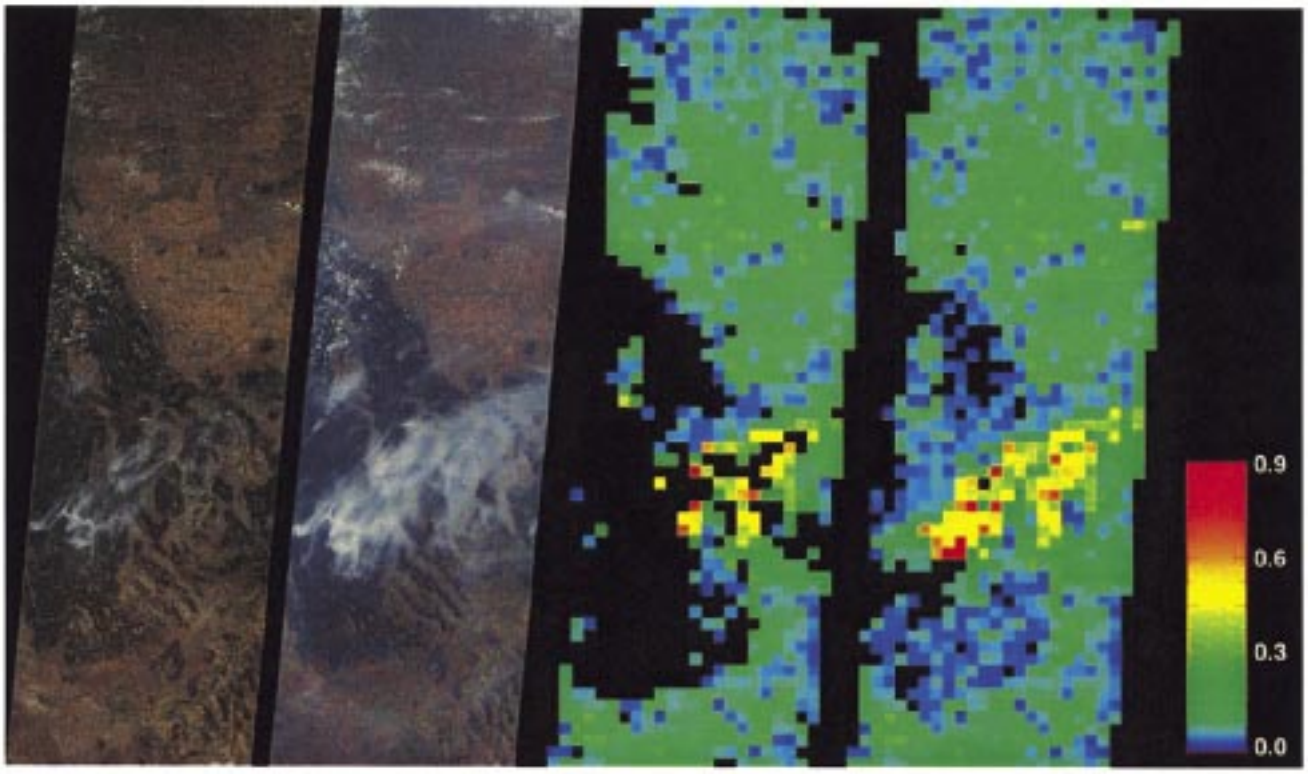

Fig. 5. Wildfires in Montana on August 14, 2000. Swath segments (path 40, orbit 3501) shown (left to right) are: true-color TOA nadir view, TOA 70° forward view, Langley ASDC-retrieved aerosol optical depth (558 nm), JPL-retrieved aerosol optical depth (558 nm).

counterparts. An exception appears to be the greater brightness of the water at the far right of the swath segment of the March nadir image, but this effect is due mainly to glint, whereas the 70° image is essentially glint-free. In general, the June images look hazier than the March ones, both over land and water, in most areas, and the optical depth maps for both dates bear out this observation.

The best fitting aerosol models for both dates are the dusty maritime variety over the water and dusty continental over land. The MISR dusty continental aerosol group is composed mainly of mixtures of sulfate/nitrate particles, and medium- and coarse-size dust, but only a single dust model from this group (75% sulfate/nitrate and 25% medium-size dust by optical depth at 558 nm) was available when these particular retrievals were performed. Additional available MISR aerosol models over land included the clean continental and industrial continental groups, both composed of sulfate/nitrate particles mixed with varying amounts of black carbon. However, it was the singular dust model that was predominately selected as the best fit in the retrieval process.

It is interesting to note that the optical depth continuity is very good going from land, across the water, and back over land again, even though two quite different retrieval algorithms and two distinct groups of aerosol models were used, depending on the type of underlying surface. Another interesting feature to note is the isolated region of large optical depth in the upper far right of the March optical depth map. Although a comparison of the nadir images for the March and June dates indicates little or no difference at this location, the 70° view March image clearly shows a distinctly brighter area there than the 70° view June image, indicating a pronounced dust cloud. This is a good example of how extreme off-nadir imagery can intensify atmospheric features, which are not obvious in a standard nadir view and the ability of the Heterogeneous Land Algorithm to detect and analyze them.

D. Wildfires in Montana

There were numerous incidents of wildfires in the western part of the United States during the summer of 2000. On August 14, 2000 (path 40, orbit 3501) MISR observed a number of wildfire smoke plumes in the Salmon River area of Idaho and extending across the Bitterroot Mountain range into southwestern Montana. True-color swath segments for this region in the nadir and 70° forward views are shown in Fig. 5. The light color areas are plains and valleys with minimal green vegetation whereas the darker areas are more vegetated mountainous terrain (not burn scar areas, which are on a much smaller scale in these images). As expected, the smoke plumes from the various fires are much more obvious in the 70° view image. Also displayed are two versions of the retrieved aerosol optical depth. The one on the left shows results from the Heterogeneous Land Algorithm which is scheduled to run at the Langley ASDC through the end of 2001. A few smoke plume optical depths are apparent but much of the mountainous terrain was designated as being too topographically complex or having too little contrast to attempt a retrieval, and these regions (including regions with unsuccessful retrievals) are displayed as black in the map.

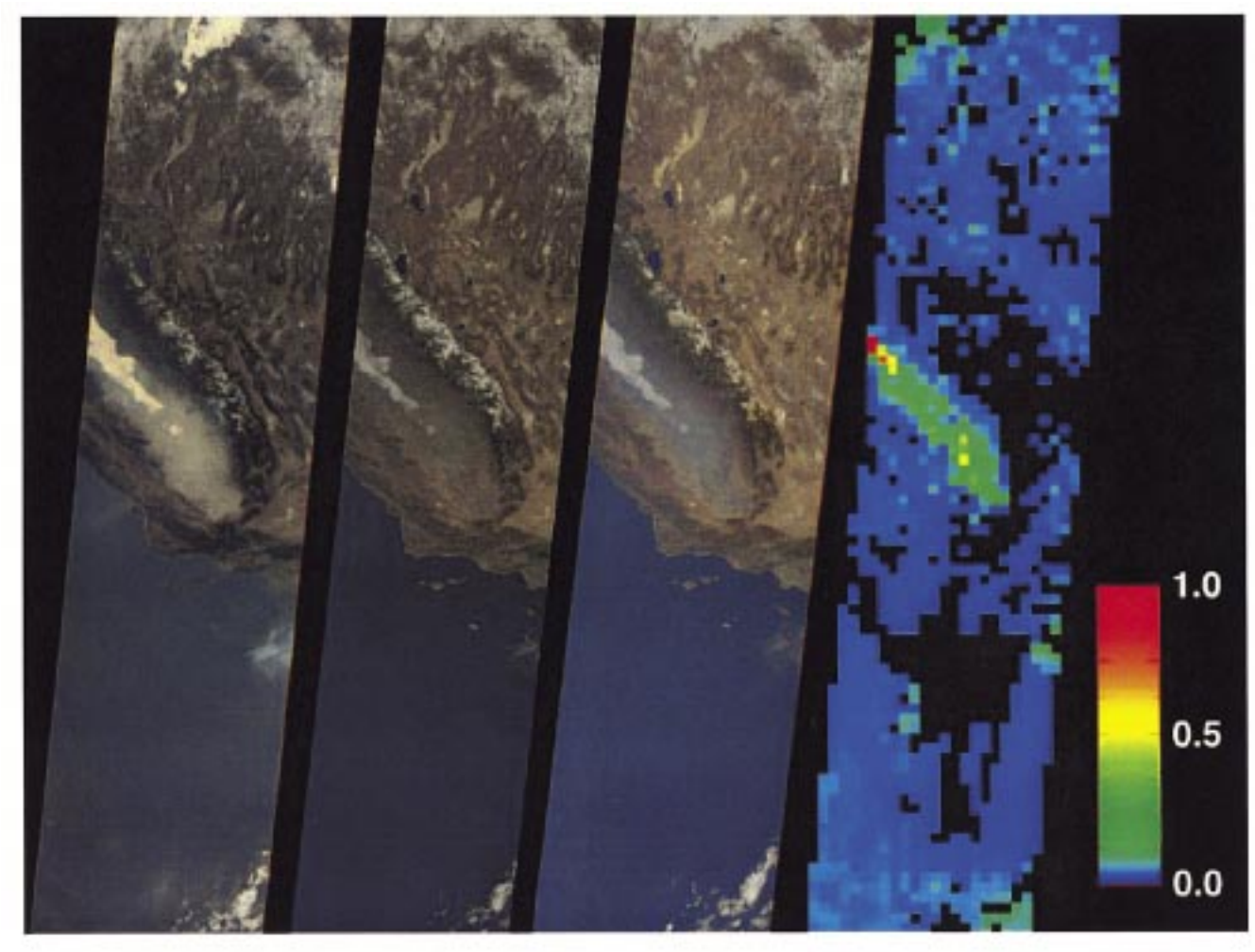

Fig. 6. Haze in central California on January 3, 2001. Swath segments (path 42, orbit 5569) shown (left to right) are: true-color TOA 70° forward view, TOA nadir view, TOA 70° aftward view, retrieved aerosol optical depth (558 nm).

The optical depth map on the right in Fig. 5 shows results from a modified version of the algorithm (run at the MISR Science Computing Facility at the Jet Propulsion Laboratory) whereby threshold conditions, as to when a retrieval is attempted over complex topographic terrain or terrain with little contrast, have been eased. A considerable increase in coverage of retrieved optical depth was achieved, showing additional smoke plume optical depths as well as optical depths for the surrounding terrain, and with no obvious detrimental effects. It can now be seen that moderate aerosol amounts (displayed as green) are mainly at the lower elevations, i.e., the Snake River valley at the bottom of the map and the Great Plains area in the upper half, whereas the blue areas, indicating less aerosol amount, are concentrated mainly at much higher elevations in more mountainous terrain. The adjustment of configurable parameters in the retrieval algorithms to increase their success rates is an ongoing task, which can only be done through considerable scrutiny and analysis of the operational processing product results.

E. Haze in Central California

A localized area of haze, situated within the San Joaquin Valley of central California, was detected by MISR on January 3, 2001 (path 42, orbit 5569). The three swath segments on the left side of Fig. 6 are true-color images for views at 70° forward, nadir, and 70° aftward, illustrating the large extent of the hazy area and the spatial contrast differences between the three images. In the nadir view, only an optically thick central tongue of fog is visible (probably the notorious "Tule" fog common to this area), whereas the 70° images, especially the forward view, show haze filling the whole valley. The retrieved aerosol optical depth map on the right in Fig. 6 covers a large region of the ocean, south of the Santa Barbara–Los Angeles coastline, extending northwards into central Nevada. There is a high degree of uniformity of a relatively small aerosol optical depth over the ocean, across the coastline, and into the continental interior. The Los Angeles basin at the far right on the coast shows little sign of aerosol buildup at this particular time of day (late morning). Within the San Joaquin Valley the turbidity was found to be considerably greater than that of the surrounding terrain. The retrieved optical depths, however, were obtained without consideration of a fog model, which has much larger particles than the sulfate/nitrate models actually used. Thus it is expected that the retrieved optical depths in the Valley may be somewhat biased on the low side. The optical depths obtained for the tongue of fog are unreliable, since

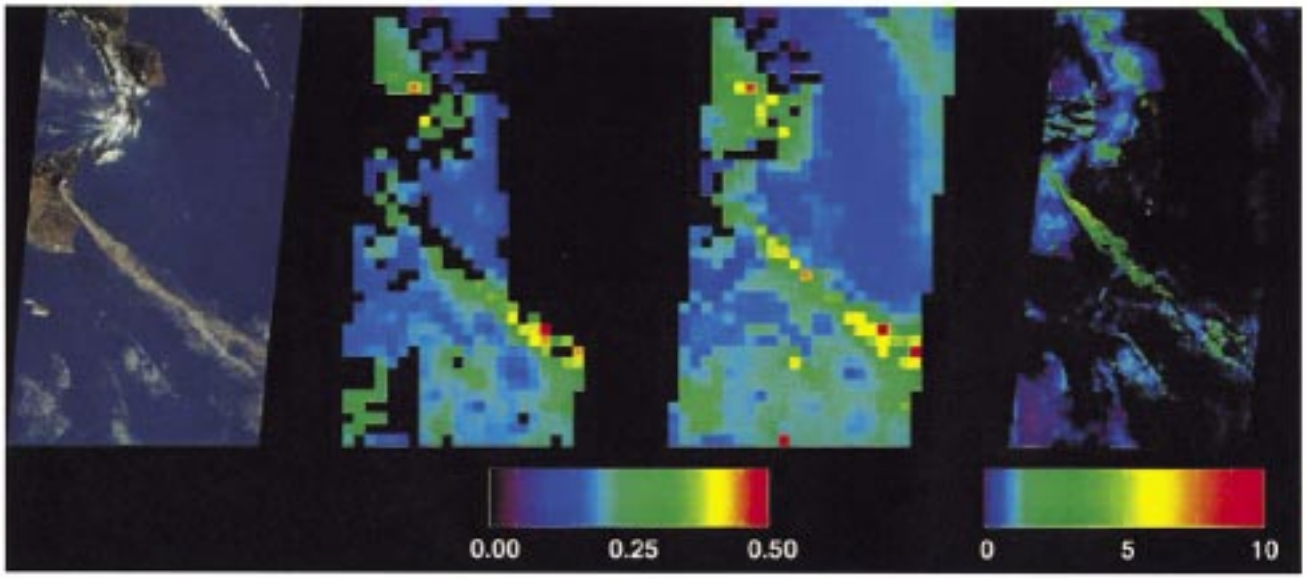

Fig. 7. Mount Etna eruption on July 22, 2001. Swath segments (path 187, orbit 8476) shown (left to right) are: true-color TOA 70° forward view, mean-retrieved aerosol optical depth (558 nm), best-fit-retrieved aerosol optical depth (558 nm), cloud/plume heights (km).

the multiangle images indicate that it is optically thick to a degree that no surface contrast can be discerned (a condition needed by the Heterogeneous Land Algorithm).

A noticeable lack of retrieval success is apparent in a large area of the ocean (black regions in map), even though the multiangle images on the left display no evidence of cloud contamination. This kind of occurrence, where all 49 ocean aerosol models have failed under clear sky conditions, has been observed on a number of occasions in various parts of the world's oceans. As explained in Section III-B, this failure is believed to be directly attributable to an inadequate choice of aerosol models with small effective radii, coupled with the high sensitivity of the MISR instrument over ocean to particle size. A similar sized region of no retrievals is also apparent on land over the Sierra Nevada mountain range. Here, however, retrievals were not attempted for the most part, due to the complex nature of the terrain.

F. Mount Etna Eruption

On July 22, 2001 (path 187, orbit 8476) MISR observed a large volcanic plume emanating from Mount Etna in Sicily. As can be seen in the 70° forward view true-color image on the left in Fig. 7, the plume is well over 300 km long, extending beyond the eastern edge of the swath segment. Two maps of retrieved optical depth are displayed in the central part of the figure. The one on the left shows the averaged results using only successful retrievals, i.e., those which satisfied the various χ^2 tests used to find the best fitting aerosol models, and the one on the right showing the results for the best fitting model only, whether or not it passed the χ^2 tests. This second version of the map essentially permits complete coverage of optical depth in a swath segment (except for detected clouds and unusable terrain), but with reduced accuracy. Thus, for instance, all the unsuccessful retrievals (colored black) in the large patch of clear sky ocean in the upper right of the right-side map have been filled with the optical depths of the best fitting, but test-failed, models. This relaxing of standards is no substitute for having better aerosol models, but it does illustrate the fact that even nonoptimum models can provide optical depth determinations that are within an acceptable range of uncertainty [5], as evidenced by a comparison of the two maps.

Optical depth retrievals along the plume length are compromised somewhat by the fact that the Dark Water Algorithm searches for and uses only the minimum radiance pixels within the 16 pixel $\times$ 16 pixel aerosol retrieval region (see Section IV-A). Thus, a region with a plume partially filling it will tend to produce an optical depth for the least contaminated pixel, which will not be representative of the plume itself. In fact, if the visibly discernible plume width is less than the dimension of the region (17.6 km), the retrieval process can miss the core of the plume entirely. For the Mount Etna plume in Fig. 7, this has likely led to an underestimate of its optical depth, the exception being that part far away from the volcano which is wide enough to accommodate up to three retrieval regions.

The map on the far right in Fig. 7 shows the heights of the terrain, clouds and plume, derived from the MISR stereo image processing [9]. It shows the plume near the volcanic vent to be at an altitude of about 5000 m above sea level, decreasing somewhat with distance from the vent, and with clouds in the scene being considerably lower. These high altitudes indicate that this particular eruption was quite powerful. Plume/cloud height information is routinely provided as part of the MISR standard products, generated and archived at the Langley ASDC.

V. Discussion

The examples described in Section IV indicate that a significant degree of success has been achieved in using MISR data to retrieve aerosol properties. Much of this success is due to fact that data from all nine view angles are routinely used, allowing observations of air masses up to three times that of nadir.

Even when scattered clouds are present in the images, the extreme-off-nadir cameras (60° and 70° view angles) can usually see a sufficient fraction of clear surface within those 17.6-km regions, which are clear in the nadir camera.

An important element in quantitatively gauging that success is through a rigorous validation effort, by which an independent characterization of the atmosphere is achieved, principally through intensive field campaigns which can provide information *in situ* on aerosol properties, and ground-based measurements made simultaneously with the space-based observations. In fact, such measurements are routinely made by a large number of sunphotometers strategically placed about the globe, and the bulk of which are associated with AERONET [10], a network of automated CIMEL radiometers coordinated by the NASA Goddard Space Flight Center. During the SAFARI 2000 dry-season field campaign in southern Africa, a large number of AERONET sunphotometers were in operation in the region, allowing a comparison of their derived aerosol optical depths with those retrieved using MISR [11]. This particular study showed very good agreement between the two sets of results, even though all the retrieval locations were situated on land. This initial validation effort has been very encouraging, but it is only the start of a larger, ongoing effort, designed to utilize the results from all AERONET sites around the globe.

None of the examples of retrieved optical depth described in this paper, however, had any available ground-based aerosol information with which to make a comparison. Instead, they were chosen to elucidate the ability of the current operational retrieval process to handle a variety of aerosol phenomena. As such, they represent a part of a larger, ongoing qualitative study of the MISR aerosol product, which is also an important aspect of the overall validation effort, supplementing the quantitative ground truth comparisons. The aerosol products in these examples have a maturity level, which is classified as "beta," implying that the associated retrieval algorithms still need to undergo extensive testing and evaluation. As some of these examples clearly demonstrate, modifications to the retrieval algorithms need to be implemented to improve both the quality and quantity of the aerosol products.

One of the more obvious conclusions, resulting from an ongoing assessment of the MISR aerosol product, is the need for better aerosol models, particularly when performing retrievals over water. The model improvements can be accomplished by having available a wider range of particle sizes and mixture ratios. The size distributions of tropospheric sulfate/nitrate aerosol particles in the SMART dataset to date have effective radii of 0.21, 0.27, 0.32, and 0.64 μm, a range too restrictive for many situations encountered in nature. The absence of any size distributions with effective radii significantly smaller than 0.2 μm was a critical factor in the failures of the retrieval process over ocean, which were noted in some of the examples described in the previous section. Sea salt particles in the SMART dataset, however, were able to provide the needed size distributions with effective radii which are larger than 0.6 μm. The next generation of the SMART dataset will be restructured to include additional size distributions of these smaller aerosol particles, down to 0.03 μm in effective radius, without significantly increasing the size of the dataset.

The concept of how aerosol models are formulated can also be modified to accommodate a wider variety of aerosol conditions. Currently, a dataset of predetermined mixing ratios are used to construct the two- or three-component aerosol models used in the retrievals [2], [12]. For the Dark Water Algorithm, however, these mixing ratios could be determined as part of the data/model fitting process using a least squares analysis. For the next processing upgrade, aerosol model modifications will be limited to the addition of the new models in the SMART dataset, while retaining the current concept of predetermined mixing ratios. These new models will certainly provide better fits to the observations, allowing more information to be gleaned from MISR data over ocean than is currently obtainable. If, after a period of analyzing the ensuing results, it is determined that some additional modeling finesse is justified, then the least squares determination of the mixing ratios will be included as part of the retrieval algorithm.

Some effort has also been made to improve the reliability of the Heterogeneous Land Algorithm. Modifications already implemented were described in Section II. Ideas for further improvement center on providing constraints to the retrievals by employing the concept that the angular signature of the directional reflectance of at least some surface types is spectrally invariant in certain wavelength regions. This is an idea developed in various forms by Flowerdew and Haigh [13], Veefkind *et al.* [14], and North *et al.* [15] and used in their analyses of data from the Along Track Scanning Radiometer 2 (ATSR-2), a two-view angle instrument. The Heterogeneous Land Algorithm in its current version assumes no relationships of any kind to connect information in different spectral bands. If, however, the idea of spectral invariance (or some other type of reliable relationship) for surface directional reflectances can be validated, then that constraint would certainly be implemented. A recently initiated comparison study of retrieved surface spectral directional reflectances, particularly for those places where the atmospheric properties are independently determined from ground-based measurements, will determine exactly what, if any, surface reflectance properties can be exploited by MISR for improved aerosol retrievals. If such improvements can be achieved, then it is expected that aerosol retrievals at considerably higher spatial resolution than 17.6 km will be feasible.

A major factor governing the success of aerosol retrievals is the issue of cloud screening. The only detection means currently used in operational processing is the implementation of the angle-to-angle smoothness and correlation algorithms described in Section III. A study of the examples of aerosol retrievals shown in the Figs. 2–7 shows that these algorithms together do a very good job of cloud detection, but careful scrutiny shows that they are not fully able to screen out all cloud activity. On the other hand, we do not want to classify volcanic and wildfire plumes as clouds. Therefore, an additional approach is currently being developed, whereby the smoothness and correlation algorithms are to be supplemented by the Stereoscopically Derived Cloud Mask (SDCM) [9] and the Radiometric Camera-by-Camera Cloud Mask (RCCM) [16]. The SDCM categorizes cloud activity based on height discrimination whereas the RCCM does so by using radiance thresholds. Agreement by the two masks that a particular pixel at a particular camera view is cloud contaminated, classifies that pixel as being Optically Thick

Atmosphere (OTA). Many OTA pixels will be comprised of cloud, but others will include thick plumes over land or ocean. As such, if there are a sufficient number of these OTA pixels in a given aerosol retrieval region, a retrieval will be attempted by assuming that the surface reflectance for these OTA pixels contributes a negligible amount to the measured radiances. Thus, the OTA Algorithm will be used as an alternative to the Dark Water Algorithm and the Heterogeneous Land Algorithm. This strategy will allow thick plumes to be more accurately analyzed, without regard to surface contrast requirements for land or minimum radiance constraints for ocean. For truly cloudy areas, this new retrieval process is expected to fail due to the inability of the aerosol models to match the spectral and angular reflectance signatures of large droplet clouds and thus would only serve to help validate that particular atmospheric condition.

Finally, the optical depth fill scheme described in Section II, used when the retrieval attempt in a region was unsuccessful, has been substantially modified. The default optical depth as the average optical depth from a nearby domain has been replaced by the optical depth of the best fitting model from a nearby region. The fill procedure is now structured such that the default optical depth of a particular region can never be propagated through more than three adjacent unsuccessful retrieval regions and usually only once. For those cases where an unsuccessful retrieval region is adjacent to regions also with unsuccessful retrievals, that region is not prescribed any type of default retrieval result and no surface retrieval is performed.

The next generation of the SMART dataset with the inclusion of new aerosol size distributions, the OTA Algorithm as a supplementary aerosol retrieval algorithm, and the improved default optical depth fill procedure algorithm were all implemented at the Langley ASDC in April 2002 (software version 2.2). Issues such as the use of spectral surface reflectance constraints in the Heterogeneous Land Algorithm and the need for a least squares determination of the aerosol type mixing ratios will be resolved during the course of 2002 and any additional algorithm upgrades in these areas should be implemented by the end of that year.

VI. Summary

Since the instrument cover first opened 18 months ago, MISR aerosol retrievals have been routinely performed at the Langley ASDC. Initial analysis of the aerosols products immediately led to some changes in the retrieval algorithms to improve both the quality and the quantity of results. Retrieval examples for various types of aerosol conditions, both over land and water, showed that in general the results are satisfactory, but that additional algorithm and aerosol model improvements are also necessary. More variety in the aerosol particle size, especially for effective radii below 0.2 μm is required and will soon be implemented. However, substantial algorithm improvements, such as adding constraints to the aerosol retrieval process over land, will need more time to fully understand what is necessary and then to implement it. Given the relatively short time that MISR has been in orbit, considerable success has already been achieved in retrieving aerosol properties and it is expected that much more will be accomplished in the near future.

Acknowledgment

A number of individuals at the Jet Propulsion Laboratory have worked diligently to create the Level 2 aerosol retrieval software for use at the Langley ASDC. In particular we want to thank D. McDonald, R. Monarrez, D. Nelson, and S. Paradise. We also want to thank the Langley ASDC for their expeditious delivery of the processed MISR data and R. Kahn for many helpful discussions and his careful reading of the manuscript.

References

[1] D. J. Diner, J. C. Beckert, T. H. Reilly, C. J. Bruegge, J. E. Conel, R. A. Kahn, J. V. Martonchik, T. P. Ackerman, R. Davies, S. A. W. Gerstl, H. R. Gordon, J.-P. Muller, R. B. Myneni, P. J. Sellers, B. Pinty, and M. M. Verstraete, "Multi-angle imaging spectroradiometer (MISR) instrument description and experiment overview," *IEEE Trans. Geosci. Remote Sensing*, vol. 36, pp. 1072–1087, July 1998.

[2] J. V. Martonchik, D. J. Diner, R. A. Kahn, T. P. Ackerman, M. M. Verstraete, B. Pinty, and H. R. Gordon, "Techniques for the retrieval of aerosol properties over land and ocean using multiangle imaging," *IEEE Trans. Geosci. Remote Sensing*, vol. 36, pp. 1212–1227, July 1998.

[3] W. A. Abdou, J. V. Martonchik, R. A. Kahn, R. A. West, and D. J. Diner, "A modified linear mixing method for calculating atmospheric path radiances of aerosol mixtures," *J. Geophys. Res.*, vol. 102, pp. 16833–16888, 1997.

[4] R. Kahn, R. West, D. McDonald, B. Rheingans, and M. I. Mishchenko, "Sensitivity of multiangle remote sensing observations to aerosol sphericity," *J. Geophys. Res.*, vol. 102, pp. 16861–16870, 1997.

[5] R. Kahn, P. Banerjee, D. McDonald, and D. J. Diner, "Sensitivity of multiangle imaging to aerosol optical depth and to pure-particle size distribution and composition over ocean," *J. Geophys. Res*, vol. 103, pp. 32195–32213, 1998.

[6] J. E. Hansen and L. D. Travis, "Light scattering in planetary atmospheres," *Space Sci. Rev*, vol. 16, pp. 527–610, 1974.

[7] C. Cox and W. Munk, "Statistics of the sea surface derived from Sun glitter," *J. Mar. Res.*, vol. 13, pp. 198–227, 1954.

[8] J. Chowdhary, B. Cairns, M. Mishchenko, and L. Travis, "Retrieval of aerosol properties over the ocean using multispectral and multiangle photopolarimetric measurements from the research scanning polarimeter," *Geophys. Res. Lett*, vol. 28, pp. 243–246, 2001.

[9] D. J. Diner, R. Davies, L. DiGirolamo, A. Horvath, C. Moroney, J.-P Muller, S. R. Paradise, D. Wenkert, and J. Zong, "Level 2 cloud detection and classification algorithm theoretical basis," Jet Propulsion Lab., Pasadena, CA, JPL Tech. Doc. D-11399, 1999.

[10] B. N. Holben, T. F. Eck, I. Slutsker, D. Tanre, J. B. Buis, A. Setzer, E. Vermote, J. A. Reagan, Y. J. Kaufman, T. Nakajima, F. Lavenu, I. Jankowiak, and A. Smirnov, "AERONET—A federated instrument network and data archive for aerosol characterization," *Remote Sens. Environ.*, vol. 66, pp. 1–16, 1998.

[11] D. J. Diner, W. A. Abdou, C. J. Bruegge, J. E. Conel, K. A. Crean, B. J. Gaitley, M. C. Helmlinger, R. A. Kahn, J. V. Martonchik, S. H. Pilorz, and B. N. Holben, "MISR aerosol optical depth retrievals over southern Africa during the SAFARI-2000 dry season campaign," *Geophys. Res. Lett.*, vol. 28, pp. 3127–3130, 2001.

[12] D. J. Diner, W. A. Abdou, H. R. Gordon, R. A. Kahn, Y. Knyazikhin, J. V. Martonchik, S. McMuldroch, R. Myneni, and R. A. West, "Level 2 ancillary products and datasets algorithm theoretical basis," Jet Propulsion Lab., Pasadena, CA, JPL Tech. Doc. D-13402, 1998.

[13] R. J. Flowerdew and J. D. Haigh, "Retrieval of aerosol optical thickness over land using the ATSR-2 dual look radiometer," *Geophys. Res. Lett.*, vol. 23, pp. 351–354, 1996.

[14] J. P. Veefkind, G. de Leeuw, and P. A. Durkee, "Retrieval of aerosol optical depth over land using two-angle view satellite radiometry during TARFOX," *Geophys. Res. Lett.*, vol. 25, pp. 3135–3138, 1998.

[15] P. R. J. North, S. A. Briggs, E. Plummer, and J. J. Settle, "Retrieval of land surface bidirectional reflectance and aerosol opacity from ATSR-2 multiangle imagery," *IEEE Trans. Geosci. Remote Sensing*, vol. 37, pp. 526–537, Jan. 1999.

[16] D. J. Diner, L. Di Girolamo, and E. E. Clothiaux, "Level 1 cloud detection algorithm theoretical basis," Jet Propulsion Lab., Pasadena, CA, JPL Tech. Doc. D-13397, 1997.

John V. Martonchik (A'01) received the B.S. degree in physics from Case Institute of Technology, Cleveland, OH, in 1964 and the Ph.D. degree in astronomy from the University of Texas, Austin, in 1974.

He is currently a Research Scientist at the Jet Propulsion Laboratory (JPL), Pasadena, CA, and has been with JPL since 1972. His experiences include telescopic and spacecraft observations of planetary atmospheres, laboratory and theoretical studies of the optical properties of gaseous, liquid, and solid materials, and development and implementation of 1-D and 3-D radiative transfer and line-by-line spectroscopy algorithms for studies of planetary atmospheres and earth tropospheric remote sensing. He has been a Co-Investigator in several NASA programs and is the Algorithm Scientist for aerosol and surface retrievals on MISR.

David J. Diner (A'01) received the B.S. degree in physics (with honors) from the State University of New York at Stony Brook in 1973 and the M.S. and Ph.D. degrees in planetary science from the California Institute of Technology, Pasadena, in 1977 and 1978, respectively.

He has been with the Jet Propulsion Laboratory, Pasadena, since 1981. He is currently a Principal Member of the Technical Staff and Leader of the Multi-angle Imaging Science Element in the Earth and Space Sciences Division. He has been involved in numerous NASA planetary and Earth remote-sensing investigations, and is Principal Investigator of the MISR experiment and its airborne counterpart, AirMISR.

Kathleen A. Crean received the A.B. degree in physics from Occidental College, Los Angeles, CA, in 1990 and and the M.S.E. degree in aerospace engineering from the University of Texas, Austin, in 1994.

She has been a Member of the Technical Staff at the Jet Propulsion Laboratory, Pasadena, CA, since 1994, working as a Software Engineer on the MISR Project.

Michael A. Bull received the B.S. degree (with honors) in computer science from the University of Maryland, College Park, in 1992 and the M.S. degree in computer science from the University of California, Los Angeles, in 1994.

He is currently providing software development support for MISR in the areas of geometric calibration and registration, and aerosol science algorithms. He has been with the Jet Propulsion Laboratory, Pasadena, CA, since 1996, working as a member of the software development team for the Multi-angle Imaging SpectroRadiometer (MISR) project.